ACS APPLIED MATERIALS & INTERFACES

RESEARCH ARTICLE

www.acsami.org

Functionalized and Postfunctionalizable Porous Polymeric Films through Evaporation-Induced Phase Separation Using Mixed Solvents

Ashok Zachariah Samuel, S. Umapathy, and S. Ramakrishnan*

Department of Inorganic and Physical Chemistry, Indian Institute of Science, Bangalore 560012, India

Supporting Information

ABSTRACT: Condensation of water droplets during rapid evaporation of a polymer solution, under humid conditions, has been known to generate uniformly porous polymer films. Similar porous films are also formed when a solution of the polymer in THF containing small amounts of water, is allowed to evaporate rapidly under air flow; this suggests that water droplets may be formed during the final stages of film formation. In the presence of added surfactants, the interface of water droplets could become lined with the surfactants and consequently the internal walls of the pores generated, upon removal of the water, could become decorated with the hydrophilic head groups of the surfactant molecules. In a series of carefully designed experiments, we have examined the effect of added surfactants, both anionic and cationic, on the formation of porous PMMA films; the films were prepared by evaporating a solution of the polymer in THF containing controlled amounts of aqueous surfactant solutions. We observed that the average size of the pores decreases with increasing surfactant concentration, while it increases with increasing amounts of added water. The size of the pores and their distribution were examined using AFM and IR imaging methods. Although IR imaging possessed inadequate resolution to confirm the presence of surfactants at the pore surface, exchange of the inorganic counterion, such as the sodium-ion of SDS, with suitable ionic organic dyes permitted the unequivocal demonstration of the presence of the surfactants at the interface by the use of confocal fluorescence microscopy.

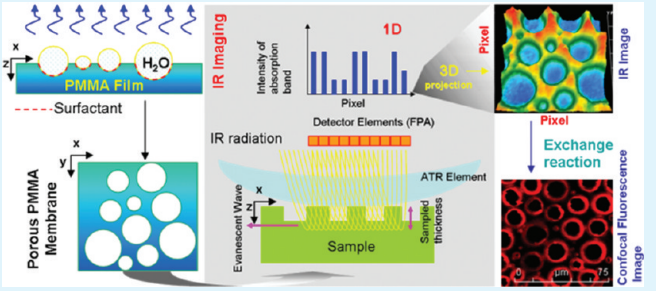

KEYWORDS: porous membranes, PMMA, surfactant, atomic force microscope, confocal fluorescence, IR imaging

INTRODUCTION

The remarkable regularity of vapor condensate pattern, formed on cold solid substrates, was demonstrated by Aitken and Rayleigh, in the early years of 20th century.[1,2] These vapor condensate patterns are commonly called "Breath Figures" — a term coined by the early explorers of this phenomenon.[3,4] Different aspects of breath-figure (BF) formation on cold solid surfaces has been explored subsequently by many researchers[5−8] and thereafter such pattern formation was also shown to occur on liquid interfaces, such as on the surface of cold liquid paraffin.[9−11] Extensive studies on experimental and theoretical aspects of the pattern formation revealed the importance of the interplay of density of liquid droplet, buoyancy, and thermocapillary convection forces at the liquid vapor interface.[9−13] One of the distinctive features of the breath-figure formation is the droplet aggregation when they come in contact.[14,15] Controlled growth of breath figures and evolution of well-ordered monodisperse patterns on paraffin oil was observed by Steyer et al.,[15] and it was proposed that formation of a thin layer of paraffin around the condensed water droplet prevented coalescence, and enabled the formation of the ordered structure.

The concept of breath-figure formation was later exploited for the generation of honeycomb morphologies in polymer films.[16] The mechanistic aspects of honeycomb pattern generation was elaborated about a decade ago[17] and subsequently a large number of papers on the preparation of porous polymeric membranes have appeared, all of which utilized the idea of water droplet condensation and thermocapillary convection.[18−20] However, very few reports have attempted the preparation of internally functionalized porous structures. One such report describes the utilization of TOPO (tri*n*-octylphosphine oxide) stabilized CdSe nanoparticle for functionalizing spherical cavities of porous polystyrene membranes.[21] During breath-figure formation, hierarchical ordering of CdSe nanoparticles takes place at the interface of the polymer solution and water droplet. It was suggested by the authors that replacement of the labile ligands attached to the nanoparticles could be a viable route to postfunctionalize the surfaces of the spherical cavities, although no experimental demonstration of this idea was discussed. Similarly, by using polymers with terminal or pendant polar groups functionalized porous films, wherein the polar groups decorate the internal pore surface, have been prepared;[22−24] here the polymer molecules

Received: October 31, 2010
Accepted: August 4, 2011
Published: August 04, 2011

ACS Publications © 2011 American Chemical Society

themselves organize in such a manner so as to drive the polar groups to the water droplet interface.

It is well-known that surfactants organize at the interface of water and an immiscible organic liquid; this behavior of surfactants could, in principle, be explored for the creation of internally functionalized porous structures. In this report, we discuss a straightforward way to generate functionalized and postfunctionalizable porous polymer films. We have employed a simple but under-utilized methodology of using a miscible solvent mixture (THF−water)[25] to generate porous polymeric membranes in a dry atmosphere. Some earlier studies[26,27] have also used relatively dry environment (R.H. 30%) to create breath-figures; here it was suggested that the recondensation of water, after fast evaporation during spin-casting of the polymer solution, as a plausible mechanism. In the present study, however, we attempt to show that it is the phase separation of water toward the later stages of THF evaporation that may be responsible for the pores in the polymer film.

MATERIALS AND METHODS

Preparation of Porous PMMA Films. Polymethylmethacrylate (PMMA) was dissolved in THF (dried over to sodium prior to use) to make 3, 4, or 5 wt % solutions. Solutions of sodium dodecylsulphate (SDS, SD Fine Chemicals) in distilled water, of desired concentrations (0.82, 8.2, and 8.66 mM), were prepared. Typically, for the preparation of porous films, 3 mL of PMMA solution was poured into a clean Petri dish followed by addition of 90 μL of the SDS solution (surfactant solution); the solution was swirled to ensure homogenization. The Petri dish containing the solution was covered with a bell jar saturated with THF vapor to effect "slow" solvent evaporation. The film preparation was carried at room temperature (30 °C) and, in one control experiment, the rate of solvent evaporation was estimated by plotting the weight loss (polymer solution + Petri dish) as a function of time. The graphical variation (see the Supporting Information S1) gave an average rate of evaporation of about 13 mg/min; clearly the slopes were higher in the beginning and slowed down later. All other films were prepared under similar conditions for this study. Cetyl trimethylammonium bromide (CTAB), Myristic acid (tetradecanoic acid), and poly(methylmethacrylate) (PMMA) were procured from Sigma-Aldrich Chemical Co. and used as received.

AFM and SEM Analysis. AFM analyses of the porous films were performed using Nanoscope IVA multimode AFM (Digital Instruments, Santa Barbara, CA). All the images presented are tapping mode height images, recorded using a tip of force constant 40 N/m. Image analyses were performed using the software provided along with the Nanoscope IVA. The porous films were first observed under a light microscope to identify the regions of the film where the largest pores are formed and this portion was cut and used for the imaging studies. The FE-SEM image was recorded using field-emission scanning electron microscope (FE-SEM, FEI Nova-Nano SEM-600, Netherlands).

IR Imaging Analysis. IR imaging was performed using 7000/7000e FT-IR spectrometer equipped with 600 UMA microscope (Varian Inc.). Liquid nitrogen cooled MCT (Mercury cadmium telluride) Focal Plane Array (FPA) detector (128 × 128) was used for recording images. Germanium (Ge) ATR-FTIR (15x) accessory with an outer ray incident angle of 50° was used to perform imaging. ATR-FTIR imaging was done using 64 × 64 pixels at the center of the FPA such that each pixel, in ATR-FTIR imaging mode, is optimized to image an area of ~1 μm^2. At 1000 cm^{-1} the spatial resolution of IR is approximately 5 μm (half of wavelength). The refractive index of Ge is 4.0 and hence the expected theoretical resolution is 1.25 μm (at 1000 cm^{-1}) and at higher wavenumbers this value is smaller. However, experimentally this spatial resolution is usually not achievable. Nevertheless, the detector is optimized for the best resolution achievable (theoretically) and thus each pixel is optimized to sample an area of 1 μm^2. Therefore, in the images, 64 pixels approximately measures 64 μm^2. This scale is used for the pore size measurements. PMMA porous films were directly kept under the ATR crystal and imaging is performed by keeping the film in close contact with ATR crystal.

Dye-Exchange Reaction. The porous films were immersed directly into an aqueous solution of Rhodamine B (100 mL of 15 mM, solution; 2 mL acetonitrile was added to improve wetting). The solution was sonicated for 30 min to effect better interaction between PMMA film and solution. The film was removed from the solution and washed thrice with distilled water (under sonication) and dried.

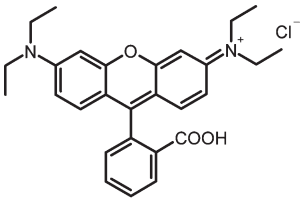

Rhodamine B

Confocal Fluorescence Microscopy. Fluorescence imaging was carried out using a Leica SP5-AOBS confocal laser scanning microscope attached to a Leica DM 6000 FS upright epifluorescence confocal microscope. AOBS (Acoust-Optical Beam Splitter) automatically adjusts to selectively reflect each excitation line and allows optimization of detection close to (and overlapping) excitation lines. The system is equipped with resonance scanning stage for image acquisition. Water immersion (20x) objective of numerical aperture (N.A) 1.0 and a 10 mW solid-state yellow laser (561 nm) was utilized to record the confocal fluorescence microscopic images.

RESULTS AND DISCUSSION

As mentioned in the Introduction, one of the approaches to generate porous films is to use polymer solutions containing a small amount of a low-vapor-pressure nonsolvent (for the polymer), which is miscible to begin-with but would phase separate at the later stages of the evaporation process; this could lead to the formation of small droplets of the high boiling solvent. These droplets would eventually evaporate leading to the formation of porous polymer films. On the basis of this premise, PMMA solutions (3, 4, or 5 wt %) in THF containing small amounts of water (~90 μL) was chosen as the system for the present study. This system has the following notable features: THF and water are completely miscible and their volatility is significantly different; this causes THF to evaporate faster compared to water during the early stages. Owing to the low polymer concentration, phase separation of water and the polymer solution would occur only toward the final stages of evaporation causing the formation of water-droplets. It may, therefore, be expected that use of an aqueous surfactant solution, instead of pure water, as the nonsolvent would enable one to functionalize the inner surface of the pores because of the strong tendency of surfactants to organize at the aqueous−organic interface. To explore this idea, two different surfactants, namely sodium dodecylsulfate (SDS) and cetyl trimethylammonium bromide (CTAB), were used for this study in order to generate anionically and cationically charged internal surfaces, respectively. Porous films were typically prepared by casting 3 mL of polymer (PMMA)

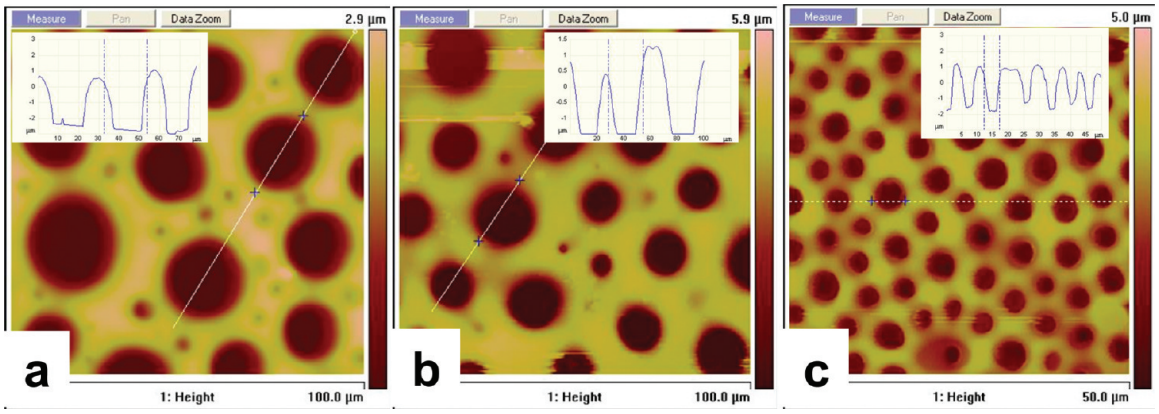

Figure 1. AFM images showing pore size dependence on SDS concentration: (a) 0.82, (b) 8.2, and (c) 8.66 mM of SDS in water. Line profiles (along the lines indicated in image) are given as insets in the corresponding images. The average pore sizes are 23, 19, and 4 μm for a, b, and c, respectively. The very small pores were not included for the calculation. Note the different image area in c.

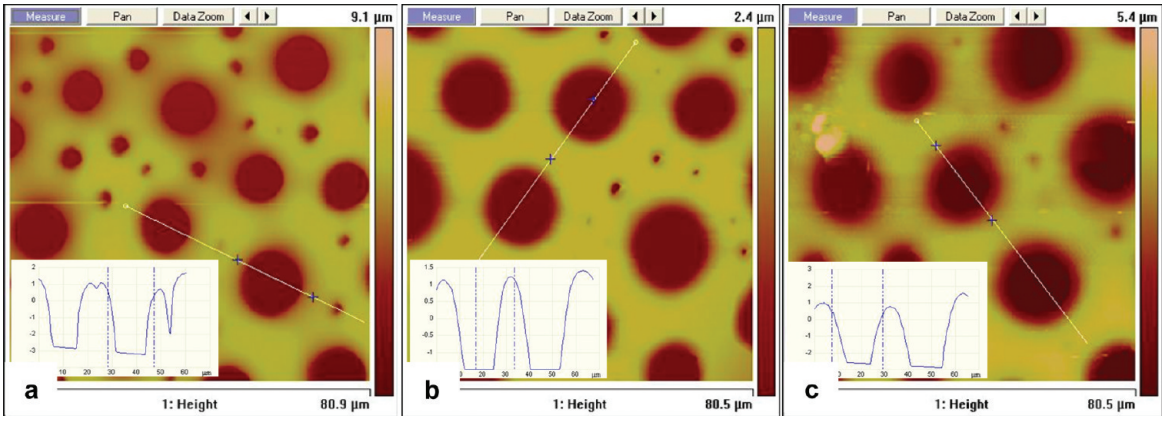

Figure 2. AFM images showing the effect of volume of surfactant solution added (8.2 mM SDS solution) on the formation of pores in the PMMA (5% solution of PMMA in THF) film. (a) 120, (b) 150, and (c) 180 μL of SDS solution. The average pore size found to increase with the volume of surfactant solution added: (a) 16, (b) 20, and (c) 23 μm.

solution in THF (3, 4, or 5 wt %) containing measured quantities of the desired aqueous surfactant solution (90 μL); the concentration of the surfactant was varied in different experiments. Representative AFM images of porous polymer films formed using different SDS concentrations are shown in the Figure 1. We also studied the formation of porous structures under different environments, such as under a bell jar saturated with THF vapor, under dry nitrogen (purge), or in the open, under ambient conditions. The porous structures formed under these different conditions were not significantly different, except when hot airflow was used (hot air dryer); the pore sizes under these conditions were significantly smaller (see the Supporting Information, Figure S2). These observations suggest that water-droplet recondensation may not be the primary cause for pore formation. An alternate mechanism of pore formation could be envisaged as follows. THF being a more volatile solvent evaporates faster causing the residual solution to become richer in water. Toward the final stages of the evaporation, water presumably phase separates from the concentrated polymer solution forming small droplets, the interface of which becomes lined with the surfactants. The presence of surfactant helps further stabilize the phase separated water droplet. Furthermore, at this stage, some of the polymer molecules are also likely to precipitate at the water droplet interface, consequently retarding the droplet coalescence. The average size of these droplets would expectedly depend on both the surfactant concentration as well as on the quantity of water present. Control experiments suggest that in the absence of added surfactant the polymer films do not form a regular porous structure. Similar experiments were carried out using the cationic surfactant, CTAB, which also lead to the formation of similar porous polymer films. However, when salts of long-chain aliphatic carboxylic acids were used as the surfactant, irregular pores were formed possibly reflecting their ineffectiveness in stabilization of water droplets (see Figure S3 in the Supporting Information). Figure 3 presents a schematic description of the various stages during the formation of the porous film; 3a represents the initial completely miscible solution of the polymer and surfactant in water-THF, 3b shows the early stages of water-droplet formation with surfactant molecules lining the interface, along with some polymer precipitation, 3c depicts the later stages after complete loss of THF and finally in 3d, the evaporation of the water leaves behind the functionalized porous PMMA film.

Effect of Surfactant Concentration. Three different concentrations of the SDS solution (0.82, 8.2, and 8.66 mM; cmc of SDS is 8.2 mM) was used to probe the effect on the pore formation.

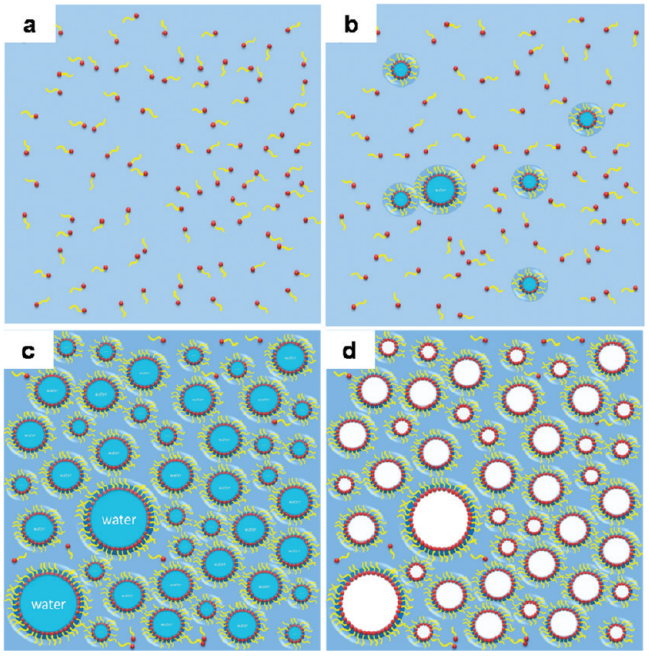

Figure 3. Postulated mechanism for pore-formation. (a) Schematic depiction of a homogeneous polymer solution (sky blue) in THF–water; yellow lines with red dots depicts dissolved surfactant molecules. (b) Initial stages of water droplet formation that are stabilized by surfactants. At this stage some polymer precipitation may also occur at the interface (depicted by the dark ring around the droplet). (c) Some droplet coalescence and continued formation of new water droplets leads to a slightly broad size distribution (coalescence and redistribution could be retarded due to the high solution viscosity). (d) Complete removal of THF followed by water generates the internally functionalized porous structures.

AFM images of the porous PMMA films, obtained using the slow evaporation process, are shown in the Figure 1; it is evident that as the concentration of surfactant increases the average pore size decreases. Line scans across the pores clearly reveal that the average pore size decreases from 23 μm (at 0.82 mM SDS) to about 4 μm (at 8.66 mM SDS); the latter concentration was above the CMC of SDS. This suggests that increasing the surfactant concentration assists the creation of larger interfacial area, consequently leads to the formation of smaller pores. Along with the reduction of the pore size, the pore size distribution was also found to improve at higher concentrations of surfactant, in particular, at a concentration above CMC. It is also seen that at low surfactant concentrations, there appears to be a bimodal distribution of the pore size; the smaller pores were typically about an order of magnitude smaller. The exact reason for their formation is still a matter of speculation, although one possibility may be that these represent openings to underlying pores; this speculation is based in SEM observations (Figure 4) that appear to indicate interconnectedness of pores. A similar reduction in pore size with increase in concentration of surfactant was also seen in case of CTAB (Figure 5). The average pore size estimated from the AFM images, of films prepared under different conditions, is listed in Table 1. In a separate experiment, the volume of the surfactant solution (at a fixed concentration) was varied to examine the influence of relative volume of surfactant solution; a smaller but significant increase in pore size with increase in surfactant volume is noticed (Figure 2), although the increase

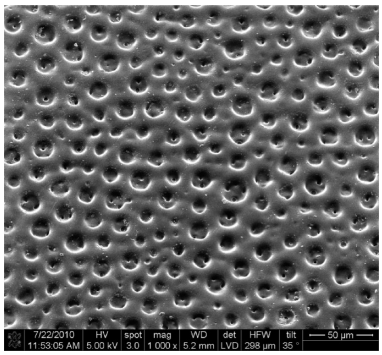

Figure 4. Field-emission scanning electron microscope (FE-SEM) image of the porous membrane prepared using SDS solution of 8.2 mM concentration.

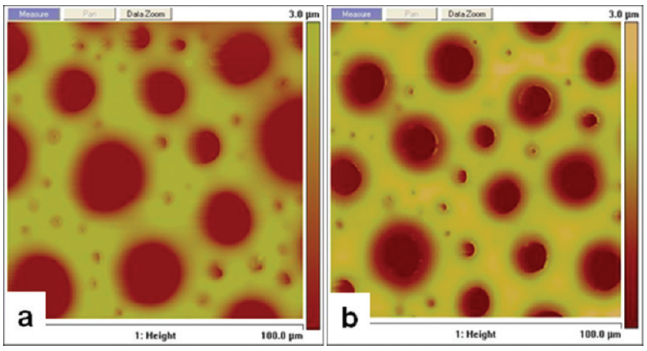

Figure 5. AFM images showing difference in pore size of the PMMA film formed at two different concentrations of CTAB solution in water: (a) 8.2 and (b) 12 mM.

Table 1. Effect of SDS Concentration (in water) on the Pore Size; Values Were Estimated from AFM Images (σ, standard deviation)

sample	conc. of surfactant (mM)	avg pore size[a] (μm)	σ
PMMA-THF-SDS-H_2O	0.82	23	4.0
	8.2 (CMC)	19	2.8
	8.66	4	0.5
PMMA-THF-CTAB-H_2O	8.2	25	8
	12	17	3

[a] Pore size refers to width (diameter).

gets smaller at higher volumes of surfactant solution. It is, therefore, evident that both the surfactant concentration and the relative volume fraction of the surfactant solution govern the size of the pores formed; at least within the window of the variation made during this study. In an effort to understand this further, the cloud point of the polymer solution in THF (3 wt %) was estimated by gradually adding increasing amounts of water (i.e., SDS solution); in other words the volume of water (or surfactant solution) required to cause a visible turbidity was determined (see the Supporting Information, S4). These measurements revealed that phase-separation is clearly facilitated in the presence of SDS, whereas the onset point did not appear to depend on the surfactant concentration. On the basis of these experiments, it was difficult to draw any concrete conclusions, as

the turbidity may originate either because of water droplet formation or polymer precipitation. Evidently, the mechanism of pore formation in the presence of the four components, namely, water, THF, surfactant, and polymer, is complex and the simplistic explanation we have provided may not capture the entire essence; however, it is clear that increase in surfactant concentration does lead to a decrease in the average pore size. Further experiments are clearly needed to fully understand the mechanistic nuances.

IR Imaging Studies. ATR-IR spectroscopic imaging works on the principle of attenuation of evanescent wave due to sample absorption.[28] The presence of a high refractive index ATR element, such as Ge, helps improve the spatial resolution. The porous structures formed in the polymer film are adequately large to be resolved in IR imaging experiment. From AFM studies, the typical depths of the pores were estimated to be larger than 3 μm in most of the cases. The depth of penetration of a 5.8 μm IR radiation (1723 cm^{-1} wavenumber) in PMMA film was estimated to be around 0.34 μm.[29] In the figure 6, the major components of the IR imaging system (ATR element, sample and the detector) is pictorially represented. The IR radiation from the source (e.g., Globar) is passed through an ATR element (e.g., Ge, as objective in the microscope) in order to improve the spatial resolution of the image. When the angle of the incident beam is above the critical angle, total internal reflection takes place and as a consequence an evanescent wave gets generated. As mentioned earlier, the evanescent wave extends a few micrometers (the exact value depends on the wavelength of IR) off the surface of the crystal. When the sample is kept in contact with the crystal, this evanescent wave serves as the IR source for obtaining the spectrum. Depending on the refractive index of the sample, the depth of penetration of the evanescent wave is modulated; this permits effective sectioning of the top surface of the sample. Absorption by the sample attenuates the reflected radiation from the ATR, which upon spatial resolution by a pixilated focal plane array detector (only one row is shown) enables one to obtain a spatially resolved IR spectrum of the sample. The intensity of absorption band at each pixel would be a function of concentration of the sample in the corresponding spatial area. A pictorial representation of such an intensity profile is shown in the figure 6; this intensity profile generated in 2-dimensions is referred to as the '*image*'. The efficacy of ATR-FTIR spectroscopic imaging to study the surface morphological features of the porous PMMA membranes is explored in this study.

The C═O stretching vibration of the ester carbonyls in PMMA was used to image the distribution of PMMA in the porous films. The 2D (and 3D projection) intensity distribution of 1723 cm^{-1} peak (distribution of PMMA) in the 64 × 64 μm^2 area is shown in figure 7. Comparison of the measured pore sizes from AFM and ATR-FTIR images is presented in table 2. The differences in the average size may be attributed to the deformation in the sample due to close contact with the ATR crystal and

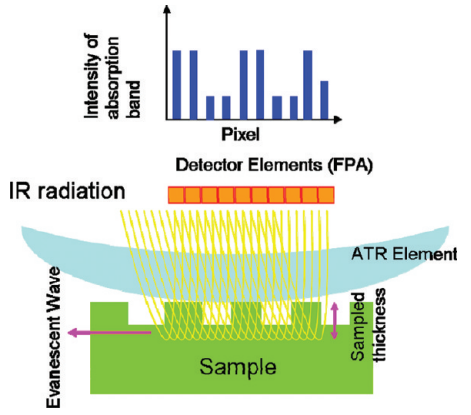

Figure 6. Schematic representation of the interaction of IR evanescent wave with the sample and the intensity profile created in FPA detector because of the variations in the sample volume in the effective sampling thickness.

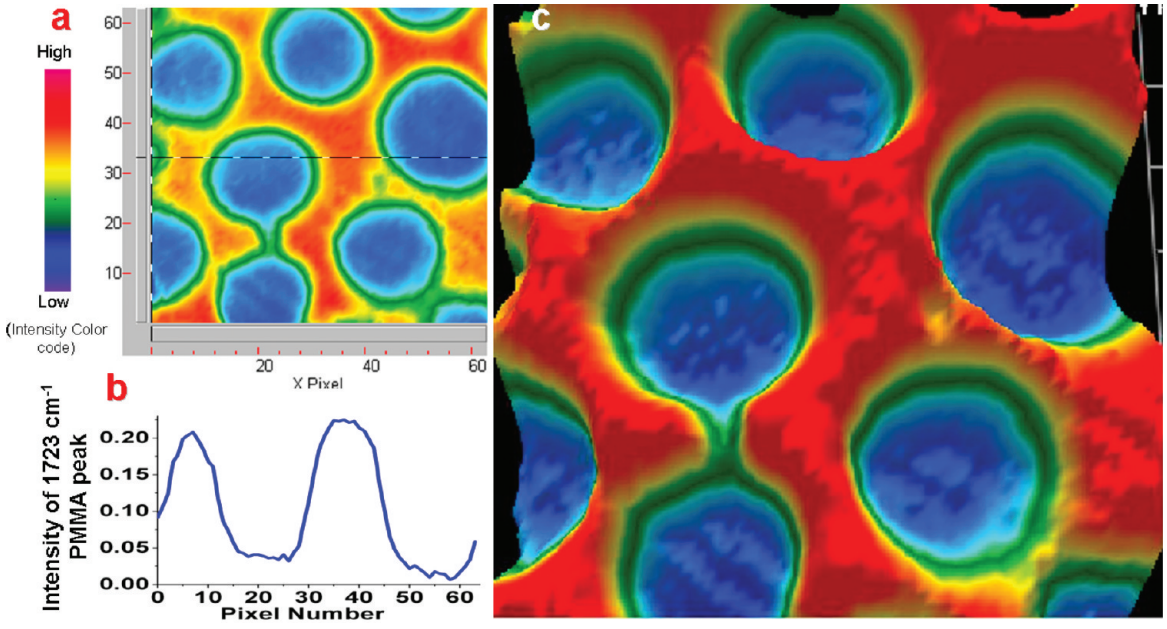

Figure 7. (a) Intensity distribution of PMMA peak 2D and c) 3D plot. Images recorded from porous PMMA film prepared using 90 μL of SDS solution in water (0.82 mM). b) The variation of the intensity of the 1723 cm^{-1} carbonyl peak as a function of moving along the dotted line (pixel position) in the image right above (line profile). The images for different surfactant concentrations are given in the Supporting Information (S6).

Table 2. Average Pore Size Estimates Using AFM and ATR-FTIR Images

system	conc of SDS (mM)	size observed in AFM images (μm)	size observed in ATR-FTIR images (μm)
THF-PMMA-SDS-H_2O	0.82	23	17
	8.2	19	13

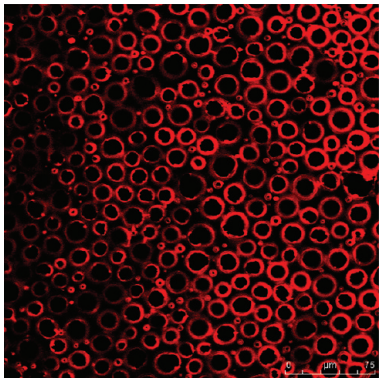

Figure 8. Confocal fluorescence image of dye-exchanged porous PMMA membrane prepared using SDS (8.2 mM) as the surfactant. The red rings indicate the regions where the dye is present, confirming that the exchange has taken place primarily at the upper boundary of the pores.

also due to the smaller sampling area. Considering the practical difficulties in mapping exactly the same area of the sample, the agreement in the average pore size is reasonable. In an effort to further probe the surface contours of the porous films, the intensity of the 1723 cm^{-1} peak as one traverses across the pore was estimated and this is plotted alongside the image in figure 7. This intensity profile matches reasonably well with the line profile obtained in AFM image, which in turn demonstrates the utility of ATR-FTIR imaging for studying such relatively large surface morphological features. However, one key aspect, namely, the presence of SDS surfactant at the pore interface, could not be inferred from the imaging study because of the low spatial resolution of this method.

Confocal Fluorescence Microscopic Studies. To gain experimental evidence for the hypothesis that pore formation in the presence of surfactants leads to the generation of internally functionalized pores, we resorted to confocal fluorescence imaging. Because the postulated mechanism for the formation of pores is through the stabilization of phase-separated water droplets by the organization of the surfactants at their interface, it is expected that the ionic head groups would decorate the internal surface of the pores. The counterions, sodium in case of SDS and bromide in the case of CTAB, are potentially exchangeable and hence they can be suitably utilized to study the nature of the interface. Thus, the exchange of the Na^+ ion with a cationic fluorescent dye would permit the selective tagging of the internal surface and consequently can be probed using confocal fluorescence microscopy. To achieve this, the SDS-based polymer films were treated with a solution of cationic dye, Rhodamine B (15 mM) and the confocal fluorescence microscopy images of the treated films were recorded. In figure 8, the fluorescence images clearly show the presence of red rings around the pore boundaries confirming the occurrence of counterion exchange. The average size of these pores were estimated and found to be around 15 μm (a broad bimodal distribution was clearly observable, see the Supporting Information, Figure S7). A control experiment was carried out with a porous film that was prepared in the absence of any surfactant and subsequently was treated with the cationic dye and its fluorescence image was recorded (see the Supporting Information, Figure S8); no fluorescence was seen. This experiment demonstrated two important points: (i) it served to confirm that the surfactants, as anticipated, are present at the pore walls, and (ii) it demonstrates the ability to exchange the inorganic counterions with organic ones, which in turn also suggests that this method could serve as an useful approach to generate variedly functionalized porous polymer films for other purposes, such as sensing, catalysis etc. 3D images of these exchanged membranes revealed a rather unexpected inhomogeneity in the dye-exchange process; the exchange appears to have occurred primarily at the upper rim of the pores. One possible reason for this limited exchange is that the surface becomes very hydrophobic after exchange with the organic dye and consequently ingress of the aqueous dye-solution into the pores is retarded. In a separate experiment dealing with paraffin wax microspheres carrying SDS on their surface, it was shown that the wetting is indeed severely retarded after the exchange of the Na ions with the organic dyes.[30] Attempts to improve the wetting by using a solution of Rhodamine B in ethanol or in a water−ethanol mixture (3:1), however, proved futile as this lead to swelling of the film, thereby causing dye diffusion into PMMA matrix; this in turn lead to images that were fluorescent over the entire film (see the Supporting Information, Figure S9). SEM measurements were also carried out to further confirm the porous nature of the films; these studies revealed that the pores may be interconnected (Figure 4), which was not evident from the other measurements. In other words, the top layer of pores appear to be interlinked with the bottom one; as alluded to earlier, the apparently very small pores seen in the AFM images may actually be openings to larger ones of the bottom layer. This is an interesting observation, as it suggests that such systems could also be used in membrane applications.

CONCLUSIONS

In conclusion, we have presented a new methodology to prepare internally functionalized porous polymeric films. This approach relies on a few simple concepts: (i) the use of a solution of the polymer in THF containing small amounts of water, that is miscible to begin with but phase separates during the final stages of THF evaporation, leads to the formation of small water droplets, (ii) the subsequent removal of these water droplets leaves behind pores in the films, and (iii) the inclusion of a surfactant in the added water leads to the selective enrichment of the surfactant molecules at the interface of the water droplet and consequently leaves behind the surfactant molecules on the internal surface of the pores, once the water is removed. The important parameters that control the size and uniformity of the pores are: (i) the surfactant concentration; it is seen that if the concentration is above the CMC of the surfactant, smaller and more uniform pores are formed, and (ii) at a fixed concentration of the surfactant, as expected, the volume of the aqueous solution added modifies the average pore size; the higher the volume of surfactant solution the higher is the average pore size. The pore size and its distribution were examined using AFM and IR imaging; AFM studies clearly reveal a distribution of pore sizes,

which typically varies from 4 to 22 μm; ATR-FTIR microspectroscopic imaging also clearly revealed the porous structure, though the spatial resolution was inadequate to demonstrate the presence of surfactants at the pore walls. Because ionic surfactants were used for this study, simple ion-exchange with oppositely charged organic dyes helped demonstrate that the pore walls are indeed decorated by the surfactant molecules; confocal fluorescence microscopy clearly revealed the presence of dye molecules at the pore surface. SEM images, on the other hand, revealed the presence of uniform pores and, in addition, it provided evidence for the presence of interpore connections between the different layers of pores. These simple experiments reveal that internally functionalized porous polymeric substrates can be readily prepared, although precise control of the pore size and distribution has been so far difficult to achieve. Further refinement of this approach, using the rich diversity of morphologies that surfactants exhibit, may enable one to create interesting porous polymeric manifolds that could find use as separation media, for gas adsorption and catalysis.

■ ASSOCIATED CONTENT

Supporting Information. Details of experimental procedures, depth of penetration calculations, and additional experimental data. This material is available free of charge via the Internet at http://pubs.acs.org.

■ AUTHOR INFORMATION

Corresponding Author
*E-mail: raman@ipc.iisc.ernet.in.

■ ACKNOWLEDGMENT

We thank IISc-Imaging Facility for access to the Confocal Fluorescence facility and Council of Scientific and Industrial Research (CSIR) for funding (scholarship to AZS). S.R. thanks DAE for the ORI award (2006-2011). S.U. thanks DST, New Delhi, for the J. C. Bose Fellowship award.

■ REFERENCES

(1) Aitken, J. *Nature* **1911**, *86*, 516.
(2) Rayleigh, L. *Nature* **1911**, *86*, 416.
(3) Baker, T. J. *Philos. Mag.* **1922**, *44*, 752.
(4) Limaye, A. V.; Narhe, R. D.; Dhote, A. M.; Ogale, S. B. *Phys. Rev. Lett.* **1996**, *76*, 3762.
(5) Merigoux, R. *Rev. Opt.* **1937**, *9*, 281.
(6) Beysens, D.; Knobler, C. M. *Phys. Rev. Lett.* **1986**, *57*, 1433.
(7) Viovy, J. L.; Beysens, D.; Knobler, C. M. *Phys. Rev. A* **1988**, *37*, 4965.
(8) Fritter, D.; Roux, D.; Beysens, D.; Knobler, C. M. *J. Stat. Phys.* **1988**, *52*, 1447.
(9) Knobler, C. M.; Beysens, D. *Europhys. Lett.* **1988**, *6*, 707.
(10) Merceroux, J. P.; Prost, J.; Gruler, H. *Nuowo Cimento D* **1984**, *3*, 204.
(11) Steyer, A.; Guenoun, P.; Beysens, D.; Knobler, C. M. *Phys. Rev. B* **1990**, *42*, 1086.
(12) Steyer, A.; Guenoun, P.; Beysens, D. *Phys. Rev. E* **1993**, *48*, 428.
(13) Stowell, M. J.; Law, T. J.; Shaw, J. *Proc. R. Soc. London, Ser. A* **1970**, *318*, 231.
(14) Family, F.; Meakin, P. *Phys. Rev. Lett.* **1988**, *61*, 428.
(15) Steyer, A.; Guenoun, P.; Beysens, D.; Knobler, C. M. *Phys. Rev. B: Condens. Matter Mater. Phys.* **1990**, *42*, 1086.
(16) Heiko, U.; Bunz, F. *Adv. Mater.* **2006**, *18*, 973.
(17) Srinivasarao, M.; Collings, D.; Philips, A.; Patel, S. *Science* **2001**, *292*, 79.
(18) Song, L.; Bly, R. K.; Wilson, J. N.; Bakbak, S.; Park, J. O.; Srinivasarao, M.; Bunz, U. H. F. *Adv. Mater.* **2004**, *16*, 115.
(19) Nishikawa, T.; Ookura, R.; Nishida, J.; Arai, K.; Hayashi, J.; Kurono, N.; Sawadaishi, T.; Hara, M.; Shimomura, M. *Langmuir* **2002**, *18*, 5734.
(20) Billon, L.; Manguian, M.; Pellerin, V.; Joubert, M.; Eterradossi, O.; Garay, H. *Macromolecules* **2009**, *42*, 345.
(21) Böker, Y A.; Chiaperini, L, K.; Horowitz, R.; Thompson, M.; Carreon, V.; Xu, T.; Abetz, C.; Skaff, H.; Dinsmore, A. D.; Emrick, T.; Russell, T. P. *Nat. Mater.* **2004**, *3*, 302.
(22) Munoz-Bonilla, A.; Ibarboure, E.; Bordege, V.; Fernandez-Garcia, M.; Rodriguez-Hernandez, J. *Langmuir* **2010**, *26*, 8552.
(23) Galeotti, F.; Calabrese, V.; Cavazzini, M.; Quici, S.; Poleunis, C.; Yunus, S.; Bolognesi, A. *Chem. Mater.* **2010**, *22*, 2764.
(24) Nystrom, D.; Malmstrom, E.; Hult, A.; Blakey, I.; Boyer, C.; Davis, T. P.; Whittaker, M. R. *Langmuir* **2010**, *26*, 12748.
(25) Park, M. S.; Kim, J. K. *Langmuir* **2004**, *20*, 5347.
(26) Wong, K. H.; Hernandez-Guerrero, M.; Granville, A. M.; Davis, T. P.; Barner-Kowollik, C.; Stenzel, M. H. *J. Porous Mater.* **2006**, *13*, 213.
(27) Poly, J.; Ibarboure, I.; Meins, J. F. L.; Hernandez, J. R.; Taton, D.; Papon, E. *Langmuir* **2011**, *27*, 4290.
(28) Griffiths, P. R.; Haseth, J. A. In *Fourier Transform Infrared Spectroscopy*, 2nd ed.; John Wiley & Sons: New York, 2007; Chapter 15, p 324.
(29) Popov, V. Ya.; Lavrent'ev, V. V. *J. Appl. Spectrosc.* **1980**, *32*, 193.
(30) Samuel, A. Z.; Umapathy, S.; Ramakrishnan, S. Unpublished work.